Precambrian Research 408 (2024) 107418

Contents lists available at ScienceDirect

Precambrian Research

journal homepage: www.elsevier.com/locate/precamres

50th Anniversary Invited Review

Prolonged parallel chronology of distinct TTG types in the Lake Inari terrain, Arctic Fennoscandia: Implications for a stationary plume-related source

Kumar Batuk Joshi [a], Jaana Halla [b,*], Matti Kurhila [c], Esa Heilimo [d]

[a] Solid Earth Research Group, National Centre for Earth Science Studies, India
[b] Geosciences Unit, Finnish Museum of Natural History, University of Helsinki, Finland
[c] Geological Survey of Finland, Finland
[d] Department of Geography and Geology, University of Turku, Finland

ARTICLE INFO

Keywords:
Archaean
High-HREE TTG
Low-HREE TTG
Porphyritic granitoid
U–Pb geochronology
Stationary mantle plume

ABSTRACT

Revealing Archaean crust-formation processes requires understanding of geochemical and chronological differences in granitoids. During the early evolution of Earth's felsic crust, large amounts of tonalite-trondhjemite-granodiorites (TTGs) were formed, making up most of the Archaean crust preserved until today. TTGs have two geochemical endmembers, the low-HREE and high-HREE (heavy rare earth elements) TTGs. The genesis of TTGs has been explained by the dehydration melting of basaltic crust, but the formation of the different types of TTGs is a subject of debate. This study provides new U–Pb zircon ages for deciphering the temporal relationships between the different TTG types in the Lake Inari terrain, Arctic Fennoscandia. The interpretation of the FIRE (Finnish Reflection Experiment) 4A line shows the existence of two tectonic blocks for the terrain. Our results from zircon populations of low- and high-HREE TTGs and adjacent porphyritic granitoids show a large time spread suggesting a prolonged migmatization in the Lake Inari terrain from 2900 to 2600 Ma. This supports a long-term source of heat such as a stationary plume related to stagnant or sluggish lid -tectonics. The high- and low-HREE TTGs show parallel ages and occur intermingled, which points to a common source instead of different tectonic settings. There is no distinct age difference between the two tectonic blocks identified in the FIRE 4A seismic reflection profile. Prolonged melting episodes of thickened felsic crust produced porphyritic granites between 2650–2500 Ma. The ~ 1.9 Ga Lapland-Kola orogeny caused minor zircon recrystallization but did not influence Archaean migmatite morphology. The Lake Inari TTGs peak approximately at 2.8 Ga, i.e., 100 Ma before the formation of the suggested Kenorland supercontinent.

1. Introduction

The study on a hotly contested question on the formation of the Earth's earliest continental crust has received increasing attention among researchers. Combining geochronological results with geochemical characteristics is a prerequisite for understanding the crust-formation processes in the Archaean. Rapidly developing geochronological and geochemical methods have provided a wealth of information about the evolution of the Earth's crust. Secular shift from sodic to more potassic in the age-constrained geochemical data for felsic crust have been interpreted to signify important geodynamic changes in the late Archaean (e.g., Condie et al., 2024; Halla, 2018; Joshi et al., 2017, 2021; Sotiriou et al., 2023). On a global scale, Condie et al. (2024) divided the evolution of the Earth's felsic crust into three main intervals based on integrated geochronological and geochemical data: 1) 4.0–2.5 Ga, 2) 1.8–1.0 Ga, and 3) 1.0–0 Ma. The first Archaean interval is characterized by TTGs showing low LILE (large-ion lithophile elements), HFSE (high field strength elements) and REE (rare earth elements).

Dating the tonalite-trondhjemite-granodiorites (TTGs), the major Archaean crust-forming rocks (e.g., Moyen and Martin, 2012) and detrital zircons have provided a global timeframe for the growth of Archaean continental crust (e.g., Joshi et al., 2022a and references therein). Compared with the Proterozoic and Phanerozoic cyclic supercontinent formation and breakup producing a few significant peaks of crustal growth, the Archaean crust formation was more continuous, albeit episodic (Joshi et al., 2022a). TTGs were formed continuously

* Corresponding author.
E-mail address: jaana.halla@helsinki.fi (J. Halla).

https://doi.org/10.1016/j.precamres.2024.107418
Received 7 January 2024; Received in revised form 30 April 2024; Accepted 1 May 2024
Available online 17 May 2024

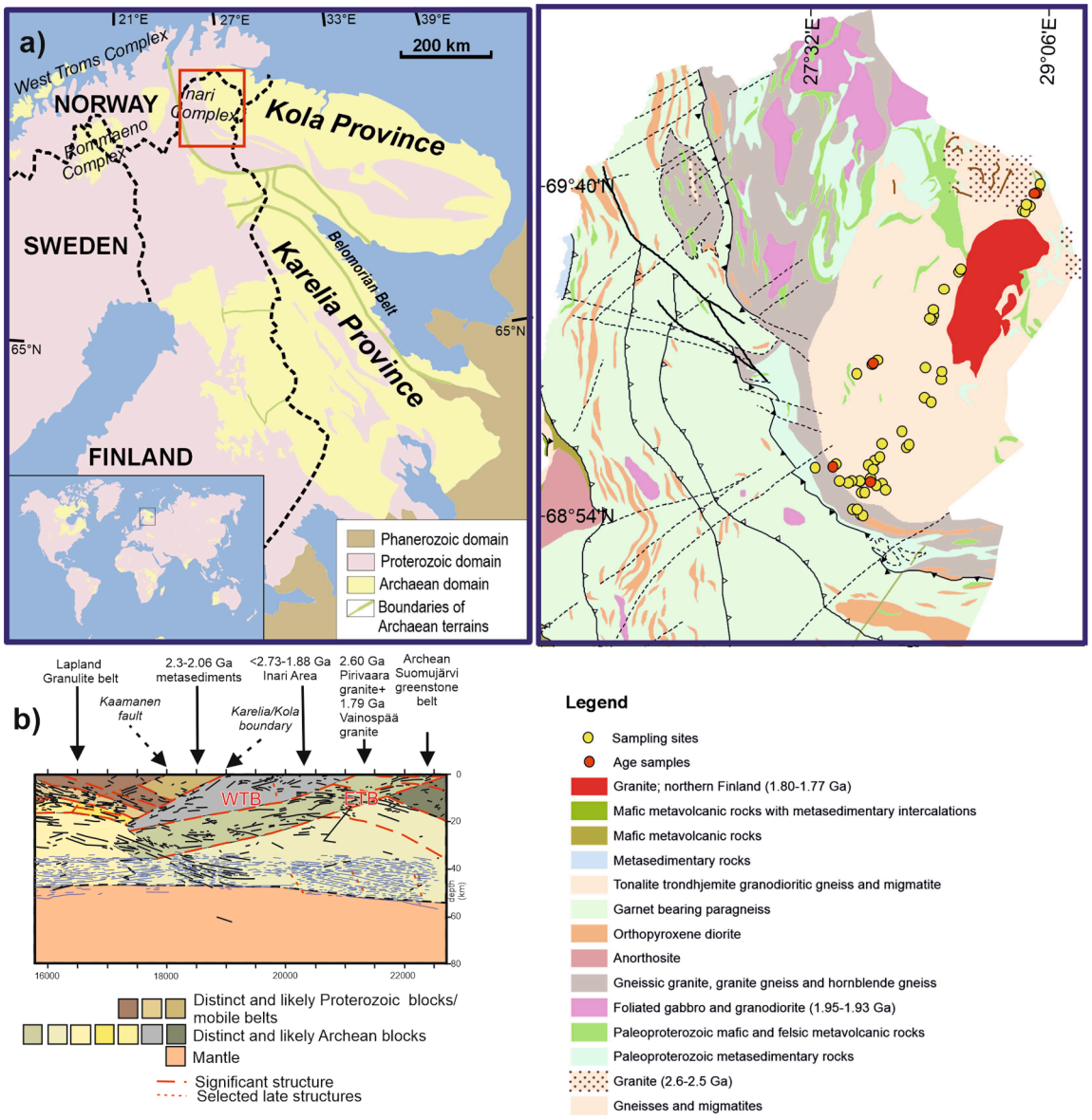

Fig. 1. (**a**) Simplified Fennoscandian map showing the study area (left). Sample locations in the islands of Lake Inari and along the Kaamanen-Näätämö road (FIRE 4A) in the western margin of the Kola craton, northern Lapland (right). Red circles indicate geochronological and yellow circles geochemical (data in Halla et al., 2024) sample locations. (**b**) Relevant part (Inari-Näätämö) of the interpretation of the FIRE 4A after Patison et al. (2006). Two Archean blocks (WSB = Western Tectonic Block; ETB = Eastern Tectonic Block) can be identified between Kaamanen and Näätämö.

from Eoarchaean to Neoarchaean, indicating a different geodynamic setting with more frequent but lower crustal growth peaks (Joshi et al., 2022b). Between 2.8–2.7 Ga, in the Neoarchaean, a particularly large volume of TTGs were formed (Moyen and Martin, 2012; Rollinson, 2023), then their formation decreased at around 2.5 Ga (e.g., Li et al., 2023). The findings of Halla (2018) based on comparing the selected element compositions of Eoarchaean to Neoarchaean TTGs support that the geochemical signatures of TTGs were similar throughout the Archaean, although there are important geochemical differences within the TTGs (Halla, 2018; Halla et al., 2009, 2024; Moyen, 2011). The main differences lie in the contents of HREE (heavy rare earth elements), Mg, Sc, Y, Zn and Co, which are garnet-compatible elements.

Geochemical and geochronological correlations or their absence give constraints to the tectonic setting. According to our hypothesis, coeval and intermingled TTG groups would suggest common formation such as partial melting of a basaltic plateau, whereas spatially and temporally distinct groups could indicate melting in different tectonic sites such as the lower part of the crust or subducting slab at shallow depths. Long duration of melting would give constraints on the tectonic environment. For example, the intrusive rates of a continental arc vary over time and are characterized by short flareup events interspersed with slightly longer magmatic lulls (Ducea et al., 2015a,b; DeCelles et al., 2009). A short magmatism duration may thus indicate rapid tectonic convergence, while long duration of magmatism may be achieved in a stationary plume environment associated with stagnant or sluggish tectonics (Tarduno et al., 2023). The genesis of TTGs has been largely explained by the melting of basaltic crust and this has been well established in the literature (e.g., Moyen, 2011; Nagel et al., 2012; Moyen and Martin, 2012; Johnson et al., 2021) and attributed to subduction or plume-related tectonics.

In this study, we provide geochronological constraints on the tectonic setting of the Lake Inari terrain of the Archaean-Paleoproterozoic Lapland-Kola Province. Our research area consists of TTGs that represent both high- and low-HREE types. They enclose metabasalts and are cut by later porphyritic granitoids and occasional pegmatitic dykes. The outcrops are exposed on the islands of Lake Inari and by the road

followed by the FIRE (Finnish Reflection Experiment) 4A seismic reflection line that deciphers two blocks, the eastern (ETB) and western (WTB) tectonic block. We expect that the dating of the blocks could reveal whether they were originated in the same or different tectonic event.

We date both low- and high-HREE TTGs aiming to find out the duration of the partial melting event that generated the terrain. According to structural and geochemical studies of Halla et al. (2024), the Lake Inari terrain formed when plateau basalts converted to TTGs through a process known as mid-crustal migmatization, i.e. partial melt SEMR (segregation, extraction, migration and redistribution) processes controlled by rheological crustal strength drops at various melt fractions and synanatectic strain (Halla et al., 2024). Weinberg and Hasalová (2015) state that even in amphibolite facies conditions, water-fluxed melting, identified by the presence of peritectic hornblende (T = 675–850°C and P 4–11 kbar), can result in voluminous melting. Migration of water-rich fluids and melts from granulite-facies dehydration melting to amphibolite facies and the subsequent water-flushed melting of metabasalts could account for the formation of TTG-amphibolite terrains (Halla et al., 2020). The variable geochemical signatures of TTGs seem to reflect internal magmatic processes such as mingling of magmas that have experienced different evolutionary paths in terms of source mineralogy, degree of partial melting, differentiation and migration (Halla et al., 2024).

Our main objectives are to 1) find out the duration of the migmatization of the Lake Inari terrain to get constraints for their tectonic setting, 2) date the two geochemical endmembers of the Lake Inari TTGs to shed light on their temporal and spatial relationships and source, 3) detect the possible age difference between the two interpreted tectonic blocks of the FIRE 4A line and, 4) constrain the chronology of the Lake Inari terrain and 5) contribute to the global understanding of Archaean crustal evolution.

2. Geological setting

Our research area (Fig. 1a) is the Lake Inari terrain, an Archaean part of the Archaean-Paleoproterozoic Inari Complex, first studied by Meriläinen (1976). The Inari Complex formed during the Lapland-Kola orogeny in the northern Fennoscandian Shield in the East European Craton (Daly et al., 2006; Lahtinen and Huhma, 2019). The northernmost part of the Fennoscandian Shield located above the Arctic Circle is here termed Arctic Fennoscandia. Halla et al. (2024) described the structures and geochemistry of the terrain that consists of TTGs and metabasalt rafts cut by porphyritic granitoids.

The orogenic Lapland-Kola Province formed because two Archaean continents collided around 1.9 billion years ago. The province consists of the Paleoproterozoic Lapland Granulite Belt (LGB; Tuisku et al., 2006) and the Archaean to Paleoproterozoic Inari Complex (Lahtinen and Huhma, 2019). Subduction was directed from northeast to southwest. In the northeast, a sediment-filled foreland basin metamorphosed to granulite facies becoming the LGB and in the southwest an arc (Inari arc) was formed. Archaean rocks of Kola Craton overthrusted the overriding crust and now form the Lake Inari terrain.

The Lake Inari terrain is well exposed for a study on the islands and along the road Nr. 971 Kaamanen–Näätämö followed by the FIRE 4A line (Fig. 1b). According to Patison et al. (2006), the margin between the LGB and Inari Arc is recognized as the suture zone between the Karelia and Kola cratons. Major tectonomagmatic events ceased throughout the FIRE profile by 1.75 Ga, after the intrusion of post-tectonic Nattanen-type granites at 1.79–1.76 Ga. These granites occupy the northern end of the Lake Inari (Heilimo et al., 2009).

The Lake Inari terrain consists of TTGs and metabasalts showing variable migmatite structures, the former representing high-melt fraction diatexites and the latter low-melt fraction metatexites. The metatexite-diatexite transitions are abundant across the terrain (Halla, 2020). Halla et al. (2024) describes their structures and geochemical features in detail concluding that the metabasalts rafts, regarded as the remnants of a plume-related oceanic plateau, are metatexites suspended by diatexite melts of the TTG composition. The structures fall in five migmatite zones: the 1) protolith, 2) metatexite A, 3) metatexite B, 4) metatexite-diatexite transition and 5) massive diatexite zones. These zones defined by Halla et al. (2024) are based on the melt-fraction and syn-anatectic strain combined with rheological crustal strength drops during partial melting and partial melting processes (Chen et al., 2017).

To give the starting point of our research, Table 1 shows the previous age determinations for the TTGs and porphyritic granitoids from the Lake Inari terrain (Huhma, 2019). The ages from the lake area fall between 2.76–2.71 Ga and the granitoids show ages from 2.60 to 2.49 Ga.

Table 1
Previous U-Pb zircon geochronology of the Archaean Lake Inari Complex according to Huhma (2019).

Sample	Method	Age
Suovavaara tonalite gneiss (A227)	TIMS upper intercept age	2760 ± 19 Ma
Käräjäsaari gneiss (A576)	TIMS upper intercept age	2744 ± 27 Ma
Kuorpasaari gneiss (A167)	TIMS upper intercept age	2737 ± 9 Ma
Kittilompolo gneiss (A213)	TIMS upper intercept age	2709 ± 35 Ma
Pirivaara granite (A226)	TIMS upper intercept age	2603 ± 39 Ma
Roavvi Tievja porphyritic granite (A207)	LA-SC-ICPMS	2524 ± 8 Ma
Akulahti tonalite (A212)	LA-MC-ICPMS	2520 ± 9 Ma
Partakko granodiorite (A270)	LA-MC-ICPMS	2504 ± 10 Ma
Näätämö porphyritic granite (A113)	TIMS upper intercept age	2493 ± 35 Ma
Näätämö quartz diorite (A115)	TIMS upper intercept age	2486 ± 27 Ma

3. Methods

Zircon separation and imaging of the studied samples were carried out at the Geohouse, University of Turku, Finland. Sample preparation involved sawing the sample for the removal of altered parts followed by jaw crushing and milling approximately 3 kg of each sample. The milled samples were sieved with a 300-μm sieve followed by washing the powdered sample to remove ultra-fine particles. The remaining sample was panned for removal of the lighter fractions and the collected fractions were dried in a hot air oven. The magnetic minerals were separated from the dried sample by a hand-held magnet. The separation of heavy minerals was done using methylene iodide. Zircons were finally hand-picked under a binocular microscope. Approximately 100–120 hand-picked zircons from the heavy fractions of each sample were mounted in transparent epoxy resin and polished to expose the interiors of the crystals. Back Scatter Electron (BSE) images were obtained prior to analysis, using Phenom XL Desktop SEM equipped with a backscattered electron detector (BSD). Samples were imaged to characterize the internal structures of individual grains under a variable vacuum with no carbon coating.

The U–Pb zircon analytical work was performed at the Geological Survey of Finland (GTK) in Espoo. Isotopic data were acquired on a Nu AttoM single collector high resolution ICP mass spectrometer, coupled with a Photon Machines Excite 193 nm laser ablation system. Samples were ablated in He gas (gas flows = 0.4 and 0.1 l/min) within a HelEx ablation cell (Müller et al., 2009). The He aerosol was mixed with Ar (gas flow = 1.0 l/min) prior to entry into the plasma. Ablation conditions were: beam diameter: 25 μm, pulse frequency: 5 Hz, beam energy density: 1.40 J/cm2. A single U–Pb measurement included a 1 s pre-ablation, 20 s of He flushing, 20 s of on-mass background measurement, followed by 40 s of ablation with a stationary beam. ^{235}U was

Table 2
Whole rock geochemistry for dated samples.

Sample	L34.2	R08.1	L28.1	R07.1	R03.1	R11.1
Rock type	TTG	TTG	TTG	TTG	TTG	Porphyritic granitoid
classified as	Tonalite	Tonalite	Granodiorite	Tonalite	Tonalite	Tonalite
REE signatures	High-HREE; Eu −	High-HREE; Eu −	Low-HREE; Eu+	Low-HREE; Eu+	Low-HREE; Eu-	Low-HREE; sharp Eu
SiO_2	75.5	73.2	72.3	71.8	72.9	70.9
TiO_2	0.17	0.24	0.14	0.28	0.17	0.59
Al_2O_3	13.5	14.1	15.3	14.9	15.0	13.8
Fe_2O_3	2.01	2.72	1.55	2.84	1.66	4.49
MnO	0.03	0.03	0.03	0.03	0.04	0.05
MgO	0.25	0.53	0.41	0.74	0.40	1.07
CaO	2.70	2.53	2.15	3.30	2.15	2.77
Na_2O	4.68	4.36	4.81	4.68	5.37	4.27
K_2O	0.90	1.93	2.85	1.06	2.00	1.67
P_2O_5	0.03	0.06	0.07	0.06	0.06	0.17
Ba	335	320	1168	419	524	244
Rb	20.2	69.6	47.9	24.5	64.60	98.9
Sr	189	122	390	296	459	176
Pb	3.72	9.20	10.1	3.9	5.90	8.95
Th	4.18	13.70	3.18	0.50	4.71	8.03
U	0.89	1.08	0.2	0.30	0.85	0.71
Hf	3.51	3.97	1.07	2.22	2.07	4.91
Zr	121	121	26.5	62.2	53.5	171
Nb	6.23	10.10	1.98	3.52	4.35	7.25
Ta	0.20	0.69	0.2	0.20	<0.2	0.23
Y	22.8	19.2	2.45	3.64	5.54	8.86
Sc	5.24	5.34	2.09	4.08	2.14	6.15
V	3.00	16.6	16.1	23.10	11.5	43.1
Cr	30	30	30	30	<30	30
Ni	20	20	20	20	<20	20
Cu	20	20	20	20	<20	20
Zn	35	50	43	39	59	93
Co	1.4	4.35	3.17	5.73	2.60	7.58
La	22.2	33.3	17.6	13.5	16.7	45.0
Ce	46.8	61.6	34.4	22.0	34.5	83.2
Pr	5.48	7.01	3.92	2.23	3.78	9.46
Nd	22.0	27.4	13.1	7.83	14.50	31.3
Sm	4.67	4.97	1.67	1.21	2.72	5.08
Eu	1.34	0.83	0.73	0.74	0.53	0.69
Gd	5.09	5.12	1.62	1.24	2.39	4.44
Tb	0.80	0.72	0.18	0.16	0.33	0.53
Dy	4.60	3.65	0.56	0.78	1.54	2.14
Ho	0.87	0.79	0.10	0.14	0.25	0.37
Er	2.57	2.08	0.26	0.43	0.49	0.81
Tm	0.33	0.28	0.1	0.10	<0.1	0.10
Yb	2.23	2.01	0.20	0.30	0.4	0.60
Lu	0.31	0.30	0.1	0.10	<0.1	0.10
La/Yb_N	7.14	11.9	63.1	32.3	27.2	53.8
La/Sm_N	3.07	4.33	6.80	7.20	3.96	5.72
Gd/Yb_N	1.89	2.11	6.70	3.42	4.49	6.12
Eu/Eu*	0.84	0.50	1.34	1.83	0.62	0.43

calculated from the signal at mass 238 using a natural $^{238}U/^{235}U$ = 137.88. Mass number 204 was used as a monitor for common Pb. In an LA-ICP-MS analysis, ^{204}Hg mainly originates from the He supply. The contribution of ^{204}Hg from the plasma was eliminated by on-mass background measurement prior to each analysis. The observed background counting-rate on mass 204 was 150–200 cps and has been stable at that level over the last years. Age-related common lead (Stacey and Kramers, 1975) correction was used when the analysis showed common lead contents significantly above the detection limit (i.e., >100 cps). Signal strengths on mass 206 were typically 250,000 cps, depending on the uranium content and age of the zircon.

Calibration standard GJ-1 (609 ± 1 Ma; Horstwood et al., 2016) and in-house reference samples A382 (1877 ± 2 Ma, Patchett and Kouvo, 1986; Huhma et al., 2012), and A1772 (2712 ± 2 Ma, Huhma et al., 2012) were run at the beginning and end of each analytical session, and at regular intervals during sessions (Supplementary material Table 9). Raw data were corrected for the background, laser induced elemental fractionation, mass discrimination and drift in ion counter gains and reduced to U–Pb isotope ratios by calibration to concordant reference zircons, using the program Glitter (Van Achterbergh et al., 2001). Further data reduction including common lead correction and error propagation was performed using an in-house Excel spreadsheet by Y. Lahaye and H. O'Brien. Errors include measured within-run errors (SD) and quadratic addition of reproducibility of standard (SE). To minimise the effects of laser-induced elemental fractionation, the depth-to-diameter ratio of the ablation pit was kept low, and isotopically homogeneous segments of the time-resolved traces were calibrated against the corresponding time interval for each mass in the reference zircon. Plotting of the U–Pb isotopic data and age calculations were performed using the Isoplot/Ex 4.15 program (Ludwig, 2012). All the ages were calculated with 2σ errors and with decay constant errors. Data-point error ellipses in the figures are at the 2σ level. The $^{207}Pb/^{206}Pb$ age offset from concordant ID-TIMS ages for the reference samples does not exceed 0.5 %.

4. Results

We selected the samples for the geochronological study based on geochemistry (Table 2) and location (Fig. 1) in the Lake Inari terrain. We collected both low- and high HREE TTGs for analysis to find out their age

Table 3
U–Pb concordia ages for the Lake Inari samples.

Sample	Total grains/ spots	n	Age (Ma)	Error ± Ma	MSWD	*c/ uic/ Pb
L34.2 Kärppäsaari (01)*	89/97	19	2882	10	1.7	c
High-HREE tonalite		5	2836	5	1	c
		7	2749	14	2.6	c
		1	2701	13	3.3	c
L28 Kahkusaari (02)	83/90	8	2863	10	1.4	c
Low-HREE tonalite		10	2818	12	1.9	c
		17	2782	8	1.2	c
		10	2752	12	2	c
		11	2712	12	2	c
		4	2665	19	2.2	c
		1	2555	24	<1	c
		3	1917	15	1.7	c
R7.1 Näätämö (03.1)	85/90	1	3077	19	1.6	c
Low-HREE tonalite		14	2894	7	1.8	uic
Eastern Seismic Block		9	2892	14	2.3	c
		15	2854	11	2	c
		39	2843	7	1.6	d
		6	2771	18	<1	c
		2	2706	14	<1	c
		1	2617	18	3.7	c
R7.3 Näätämö (03.2)	79/82	1	2798	9		Pb
Porphyritic granite		4	2639	27	3.4	c
Eastern Seismic Block		44	2600	10	2.9	uic
		8	2573	16	2.3	c
		12	2536	19	2.8	uic
		1	2533	26	1.5	c
R8.1 Jääjärvi (04)	75/77	4	2813	20	4.4	c
High-HREE tonalite		21	2802	10	2.3	uic
Eastern Seismic Block		1	2774	20	<1	c
		15	2749	16	2.2	uic
		1	2704	28	3.5	c
R3.1 Aitajärvet (05)	85/95	13	2785	8	1.5	c
Low-HREE tonalite		17	2752	8	1	c
Western Seismic Block		6	2701	17	2.8	c
		3	2629	13	2.1	c
		2	2593	13	2.2	c

c = concordant age, uic = upper intercept age, Pb = $^{207}Pb/^{206}Pb$ age.
* Geochronology number in the data sheet and BSE image.

distribution and duration of the migmatization event. We included samples from both the islands of Lake Inari and along the Kaamanen–Näätämö road on the northern side, following the FIRE 4A seismic reflection profile (Fig. 1). The samples from the FIRE 4A line represent both eastern (ETB) and western (WTB) tectonic blocks. Our sample set includes both TTGs and a younger porphyritic granitoid. In the geochronological results, spot numbers in parenthesis after sample numbers refer to BSE images and analytical data sheets. The data is available in Supplementary material 1. The migmatite structures and zones (protolith, metatexite, metatexite-diatexite transition and massive diatexite zones) are according to Halla et al. (2024). Table 3 lists the interpreted U–Pb concordia ages and gives information on the number of the total analyses, zircon grains and spots as well as the errors and MWSDs. The age errors in plots are given at 2σ level and in tables 1σ. The ≥ 90 % concordant $^{207}Pb/^{206}Pb$ ages are listed in Supplementary Table 8.

4.1. Geochemistry

The geochemistry of Lake Inari TTGs is described in Halla et al. (2024). Table 2 presents the data for the dated samples. We provide new geochemical analyses for the porphyritic granitoids in Supplementary Table 3. Based on differences on their HREE patterns, the Lake Inari TTGs divide into two main groups: low-HREE and high-HREE TTGs. These groups have distinct geochemical signatures. The low-HREE group exhibits, on average, the following contents of selected elements: low HREE (4.6 ppm), MgO (0.8 wt%), Sc (3 ppm), Y (6 ppm), Zn (53 ppm), and Co (5 ppm), in contrast to the high-HREE group showing: HREE (16.3 ppm), MgO (1.6 wt%), Sc (12 ppm), Y (24 ppm), Zn (84 ppm) and Co (12 ppm).

The porphyritic granitoids range from tonalites to granodiorites according to the classification diagram of Debon and Le Fort (1983; Fig. 2a) and have high SiO_2 and broad range of K_2O contents. They show high abundances of incompatible elements such as Rb, Ba and Th as compared to the associated TTGs. The chondrite normalized REE patterns (Fig. 2b) are moderately fractionated showing LREE enrichment and HREE depletion with strong negative Eu anomalies. The geochemical data and methods for porphyritic granitoids are available in Supplementary Table 3.

4.2. Geochronological results

4.2.1. Sample L34.2 (01) Kärppäsaari – High-HREE tonalite diatexite

The Kärppäsaari migmatite outcrop (Fig. 3a) consists of both metatexites (low-fraction melts) and diatexites (high-fraction melts). The collected sample is of a high-HREE tonalite diatexite (Fig. 3b) consisting of plagioclase, quartz and biotite, which are aligned forming a clear flow-banding structure. The diatexite lies in a proximity to abundant metatexites showing layered structures of the Metatexite zone B. The zircons (150–300 μm) are colourless, subhedral to anhedral. Some grains show patchy to oscillatory zoning, and some have visible growth rims (Fig. 3c). The obtained U–Pb concordia ages for the sample are 2882 ± 10 Ma, 2836 ± 5 Ma, 2749 ± 14 Ma, and 2701 ± 13 Ma (Fig. 3d and Table 3). The $^{207}Pb/^{206}Pb$ ages (≥90 % concordant) fall in the range of 2904–1908 Ma (Table 4, Supplementary Table 8).

4.2.2. Sample L28.1 (02) Kahkusaari – Low-HREE granodiorite diatexite

The Kahkusaari outcrop (Fig. 4a) shows metatexite-diatexite transition zone structures. The sample of a low-HREE granodiorite (Fig. 4b) was collected near the contact between a flow-banded diatexite and metabasalt raft. The main minerals of the sample are plagioclase, quartz, K-feldspar and biotite. The sample shows typical TTG geochemistry with slight enrichment in potassium. The zircons (125–300 μm) are colourless and subhedral. Some grains show visible oscillatory zoning and younger rims are visible in some grains (Fig. 4c). A few grains show no growth zones. The U–Pb concordia ages (Fig. 4d, Table 3) are 2863 ± 10, 2818 ± 12 Ma, 2782 ± 8 Ma, 2752 ± 12 Ma, 2712 ± 12 Ma and 2665 ± 19 Ma. Three analysed spots from the rim are coeval and therefore, give a concordant age of 1917 ± 15 Ma. The $^{207}Pb/^{206}Pb$ ages (≥90 % concordant) fall in the range of 2885–1834 Ma (Table 4, Supplementary Table 8).

4.2.3. Sample R7.1 Näätämö (03.1) – Low-HREE tonalite diatexite

The Näätämö outcrop R7.1 (Fig. 5a) in the ETB along the FIRE 4A line consists of TTGs, metabasalts and porphyritic granitoids. The TTG sample is from a flow-banded low-HREE tonalite diatexite consisting of plagioclase, quartz, K-feldspar and biotite (Fig. 5b). The tonalite encloses a metabasalt raft with narrow bands of leucosome representing the Metatexite zone A. The zircons grains (75–300 μm) are colourless,

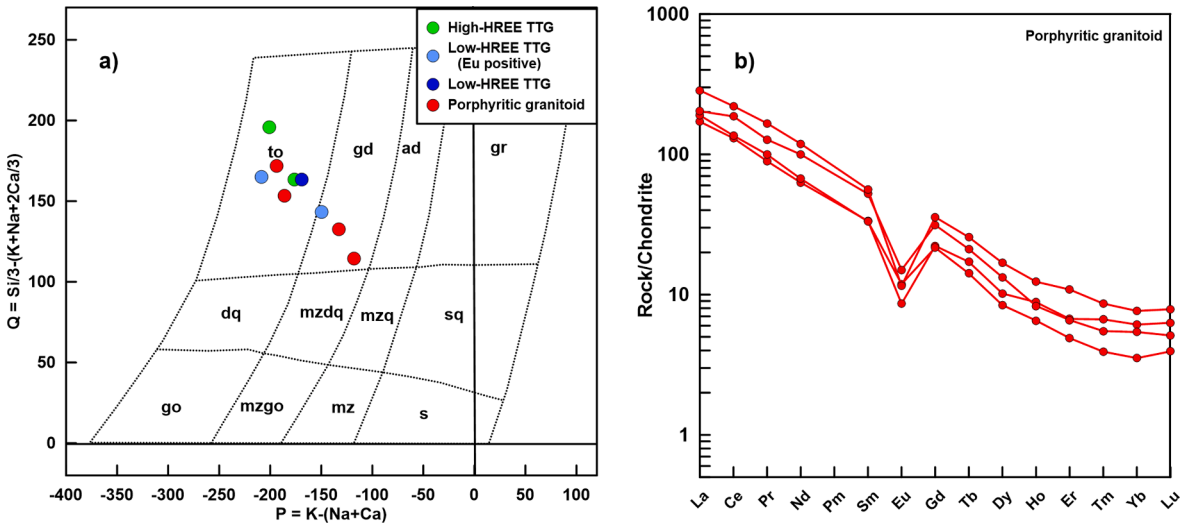

Fig. 2. (a) Classification diagram of Debon and Le Fort (1983) for the porphyritic granitoids analysed for geochemistry and for the dated TTG samples. **(b)** REE patterns for the porphyritic granitoids.

subhedral to anhedral, and show zoning from oscillatory to unzoned. A few grains show patchy zoning and inclusions are visible in some of the grains (Fig. 5c). The U–Pb concordia ages are 3077 ± 19 Ma, 2892 ± 14 Ma, 2854 ± 11 Ma, 2771 ± 18 Ma, 2706 ± 14 Ma, 2617 ± 18. The discordant analysis gives upper intercept ages of 2843 ± 7 Ma and 2894 ± 7 Ma, which are within errors of the obtained concordia ages (Fig. 5d, Table 3). The $^{207}Pb/^{206}Pb$ ages (≥90 % concordant) fall in the range of 3074–2621 Ma (Table 4, Supplementary Table 8).

4.2.4. *Sample R7.3 Näätämö (03.1) – porphyritic granitoid*

The Näätämö outcrop R7 includes also a younger cross-cutting porphyritic granitoid (Fig. 6a). The sample shows K-feldspar megacrysts in dark matrix (Fig. 6b). The zircons (150–300 μm) are colourless, euhedral, unzoned to oscillatory zoned grains with inclusions (Fig. 6c). The discordant analysis gives upper intercept ages of 2600 ± 10 Ma and 2536 ± 19 Ma, which are within errors of the obtained concordia ages. One of the zircon grains also gives an older inherited age of 2798 ± 9 Ma ($^{207}Pb/^{206}Pb$ age) (Fig. 6d, Table 3). The $^{207}Pb/^{206}Pb$ ages (≥90 % concordant) fall in the range of 2798–2480 Ma (Table 4, Supplementary Table 8).

4.2.5. *Sample R8.1 Jääjärvi (04) – High-HREE tonalite diatexite*

The Jääjärvi outcrop located in the ETB consists of tonalite diatexites in close association with metabasalt metatexites (Fig. 7a). The dated sample shows high-HREE contents and consists of plagioclase, quartz and biotite (Fig. 7b). The zircons (150–300 μm) are colourless, subhedral to anhedral, unzoned to oscillatory zoned grains with inclusions (Fig. 7c). Most ages are discordant, giving upper intercept ages of 2802 ± 10 Ma and 2749 ± 16 Ma respectively. Some of the obtained analyses give Concordia ages of 2813 ± 20 Ma, 2774 ± 20 Ma and 2704 ± 28 Ma, which are within errors to the obtained intercept ages (Fig. 7d, Table 3). The $^{207}Pb/^{206}Pb$ ages (≥90 % concordant) fall in the range of 2824–2665 Ma (Table 4, Supplementary Table 8).

4.2.6. *Sample R3.1 Aitajärvet (05) – High-HREE tonalite diatexite*

The Aitajärvet outcrop located in the WTB represents a massive diatexite (Fig. 8a). A flow-banded sample of a low-HREE tonalite consists of plagioclase quartz and biotite (Fig. 8b). The zircons (100–300 μm) are colourless, subhedral to anhedral, mostly unzoned with some showing oscillatory zoning (Fig. 8c). Removing most of the abundant discordant data points, the analysis gives concordia ages of 2785 ± 8 Ma, 2752 ± 8 Ma, 2701 ± 17 Ma, 2629 ± 13 Ma, and 2593 ± 13 Ma (Fig. 8d, Table 3). The $^{207}Pb/^{206}Pb$ ages (≥90 % concordant) fall in the range of 2824–2455 Ma (Table 4, Supplementary Table 8).

5. Discussion

In this section, we discuss the U–Pb zircon analytical results from different TTG types, FIRE 4A seismic blocks (ETB and WTB), and rock types (TTGs and porphyritic granitoids) to contribute to the understanding about the Archaean crust-forming processes and their tectonic setting. From the U–Pb geochronology of migmatite terrains we get time constraints for migmatization. The duration of the migmatization, in turn, provides clues on the tectonic processes. Fast rate would indicate a sudden change in the geodynamic setting, for example an influx of fluids triggering extensive partial melting, whereas slow rate could infer a slow change in the burial depth of the original rock and/or prolonged activity in stagnant plume settings (Chen et al., 2020; Tarduno et al., 2023).

5.1. *Later metamorphism and possible lead loss*

Recrystallization of zircon at high temperatures during metamorphism can reset most geochronometers due to Pb loss. Partial melting broadens the temperature range where zircon recrystallization and growth can occur (Taylor et al., 2019 and references therein). The age of the granulite facies metamorphism of the LGB is ca. 1.9 Ga, which could be one of the potential causes for the spectrum of ages observed in the studied TTGs. However, during the ca. 1.9 Ga Lapland-Kola orogeny, the Archaean Lake Inari terrain overthrusted onto the colliding plate as an out-of-sequence thrust nappe and thus was not buried in the granulite-facies depths. The fine-grained texture and absence of garnets in the Lake Inari metabasalts suggest that the region has not undergone high-grade metamorphism since its formation (Halla et al., 2024).

At the end of the formation period of TTGs, a reheating event caused partial melting of TTGs producing porphyritic granitoids between 2.6 and 2.5 Ga. This event is unlikely to be the cause of large-scale Pb loss, because porphyritic granitoids are found only in a restricted area and the oldest TTGs (Sample R7.1), virtually without 2.6 Ga zircons, are found in the same outcrop with the ca. 2.6 Ga porphyritic granitoid (Sample R7.3, Näätämö).

Cooling of the Lapland-Kola orogen at 1.9 Ga culminated in the intrusion of post-tectonic granites at 1.79–1.76 Ga (Heilimo et al., 2009, 2014). The ca. 1.9 Ga lower temperature metamorphism caused only minor zircon recrystallisation in the Lake Inari terrain (Lahtinen and Huhma, 2019). The tectonic event did not affect the structural morphology of the terrain or cause any widespread reworking or

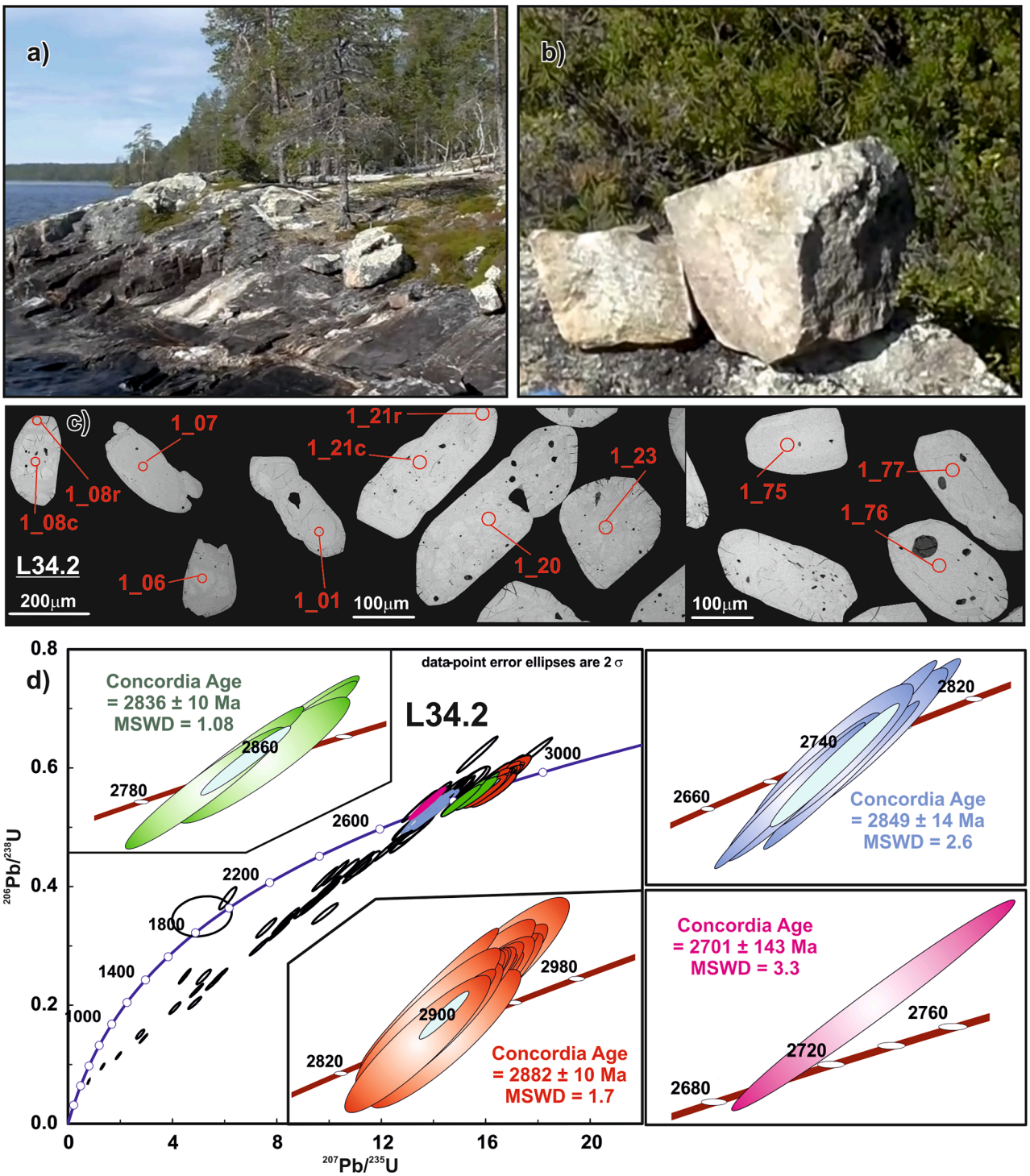

Fig. 3. Sample L34.2 (01) high-HREE tonalite, Kärppäsaari, **(a)** outcrop, **(b)** sample (diameter of the bigger sample 35 cm), **(c)** zircon BSE image, **(d)** U– Pb concordia plot. Location 68°58.540′N, 27°54.327′E. Figs. 3–8 outcrop and sample photos Pekka Kivimäki.

isotopic resetting. We confirm this by noting that the 1.9 Ga ages are recorded only in the zircon rims. This implies the preserved Archaean nature of the Lake Inari terrain.

According to Cisneros de León et al. (2021), the quasi-continuous crystallization of zircon suggests the existence of a persistent melt. Taylor et al. (2019) reported a similar age smear for the Lewisian TTGs in northwest Scotland as we obtained for the Lake Inari TTGs. They pointed out, with the help of trace element data in zircon, that a continuous spread through Neoarchaean is not due to Pb loss by diffusion but reflects a persistence of melt-bearing crust for hundreds of millions of years. Alternatively, the quasi-continuous crystallization ages, as noted in the concordia diagram, may represent discrete magmatic episodes brought on by the plume that supplied the melt (Naif et al., 2023). Therefore, we conclude that lead loss cannot explain the spread of the Lake Inari zircon ages and that the smear in zircon ages noted in the studied TTGs can be explained only by prolonged melting.

5.2. *Long-lived anatectic system*

The zircon ages recorded in the examined TTGs show a continuous

Table 4
$^{207}Pb/^{206}Pb$ ages (≥90 % concordance, *n* in parenthesis).

Age range	L34.2 (01)*	L28 (02)	R7.1 ETB (03.1)	R7.3 ETB (03.2)	R8.1 ETB (04)	R3.1 WTB (05)
>3000			3074 (1)			
3000–2850	2904–2852 (21)	2885–2853 (6)	2904–2851 (19)			
2850–2800	2843–2823 (5)	2849–2802 (14)	2849–2801 (13)		2824–2821 (2)	2802 (1)
2800–2750	2793–2760 (12)	2795–2742 (32)	2799–2758 (13)	2798 (1)	2797–2772 (3)	2797–2754 (23)
2750–2700	2746–2712 (10)	2742–2701 (15)	2737–2706 (3)		2737–2715 (3)	2747–2703 (17)
2700–2600	2698–2600 (6)	2693–2554 (10)	2696–2621 (6)	2648–2602 (6)	2665 (1)	2697–2601 (15)
2600–2500				2599–2550 (12)		2578 (1)
2500–2400				2490–2480 (2)		2455 (1)
1900–1800	1908 (1)	1944–1834 (6)				

*Geochronology number in the data sheet and BSE image.

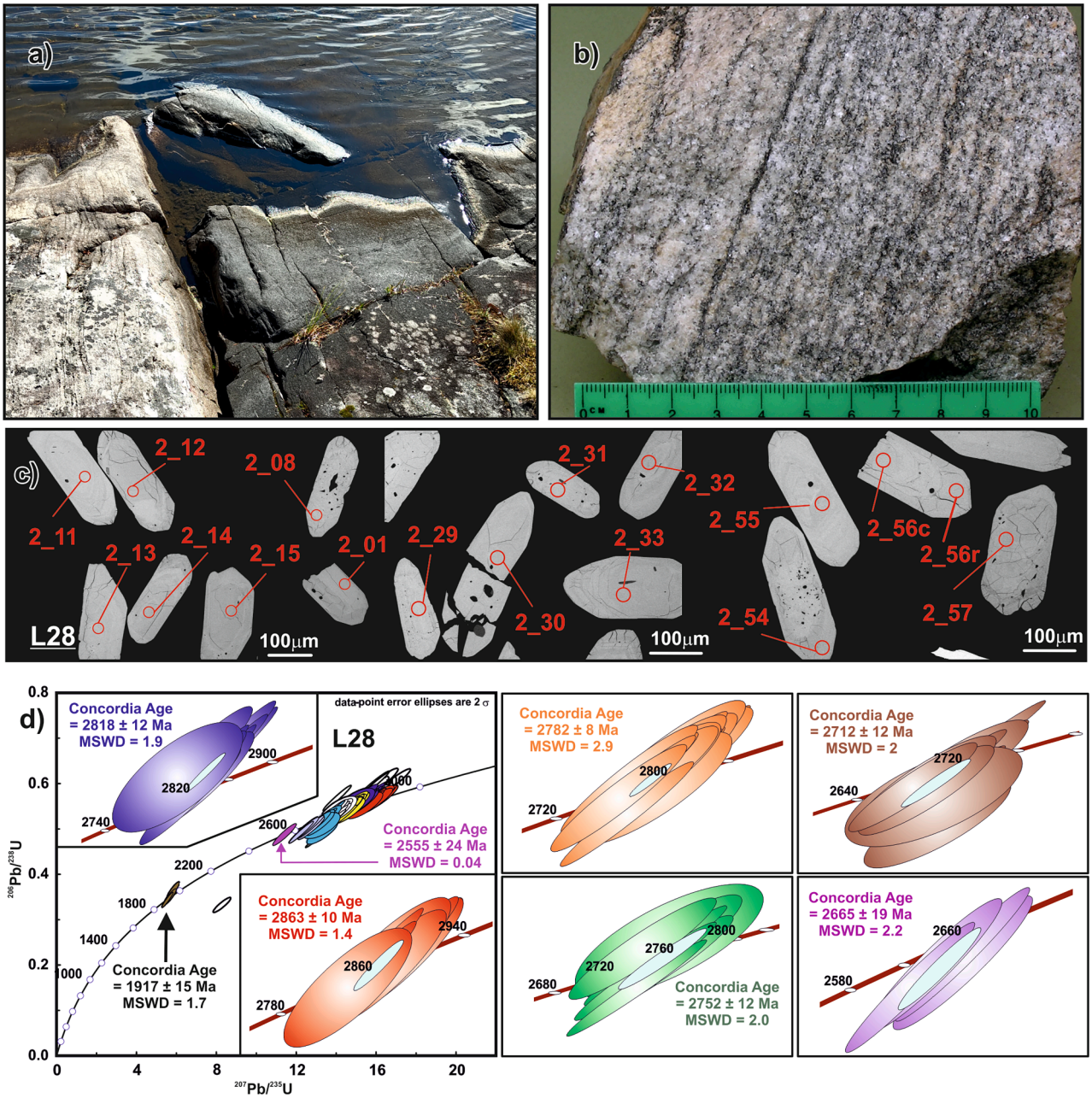

Fig. 4. Sample L28 (02), low-HREE tonalite, Kahkusaari, **(a)** outcrop (base of the photo 2 m), **(b)** sample, **(c)** zircon BSE image, **(d)** U– Pb concordia plot. Location 69°00.761′ N, 27°39.537′E.

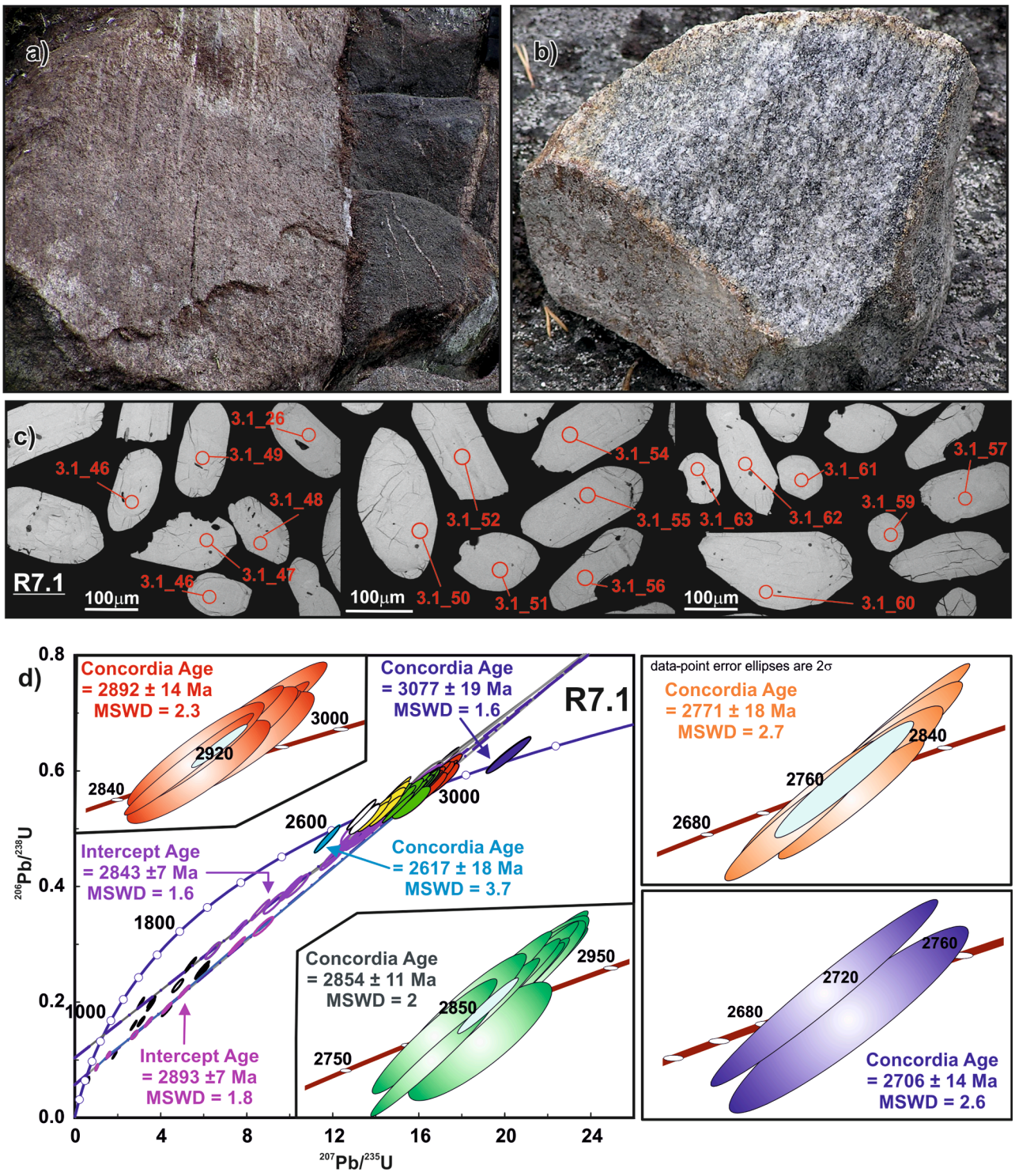

Fig. 5. Sample R7.1 (03.1), low-HREE tonalite, Näätämö, **(a)** outcrop (base of the photo 1 m), **(b)** sample (diameter 25 cm), **(c)** zircon BSE image, **(d)** U– Pb concordia plot. Location 69°39.101′N, 29°04.072′E.

spread over 300 million years, likely due to prolonged melting. The first question rising is does this age range represent several generations of melt stages (discrete melt batches) or quasi-continuous crystallisation in crust that was partially molten throughout the whole period? It would be expected that several discrete melting events would lead to geochemical evolution, but any increase in K content, for example, is not been observed before 2.65 Ga. Therefore, it is likely that the crust was quasi-molten between 2.9–2.6 Ga. The possibility of long-living existence of a such melt-bearing crust (Cisneros de León et al., 2021; Naif et al., 2023; Taylor et al., 2019) suggest that the quasi-continuous zircon crystallization ages indicate the presence of a persistent melt. According to Naif et al. (2023), melts trapped in a long-lived melt channel of distal plume origin may acquire such high volatile contents that they never freeze (depending on the depth and temperature). This fits the conception that the formation of TTGs is related to hydrated sources. Geochronological research conducted in the Lewisian gneiss terrains (Taylor et al., 2019) indicates that melt remained in the Archaean mid- to lower crust for almost 250 million years, indicating that long-lived

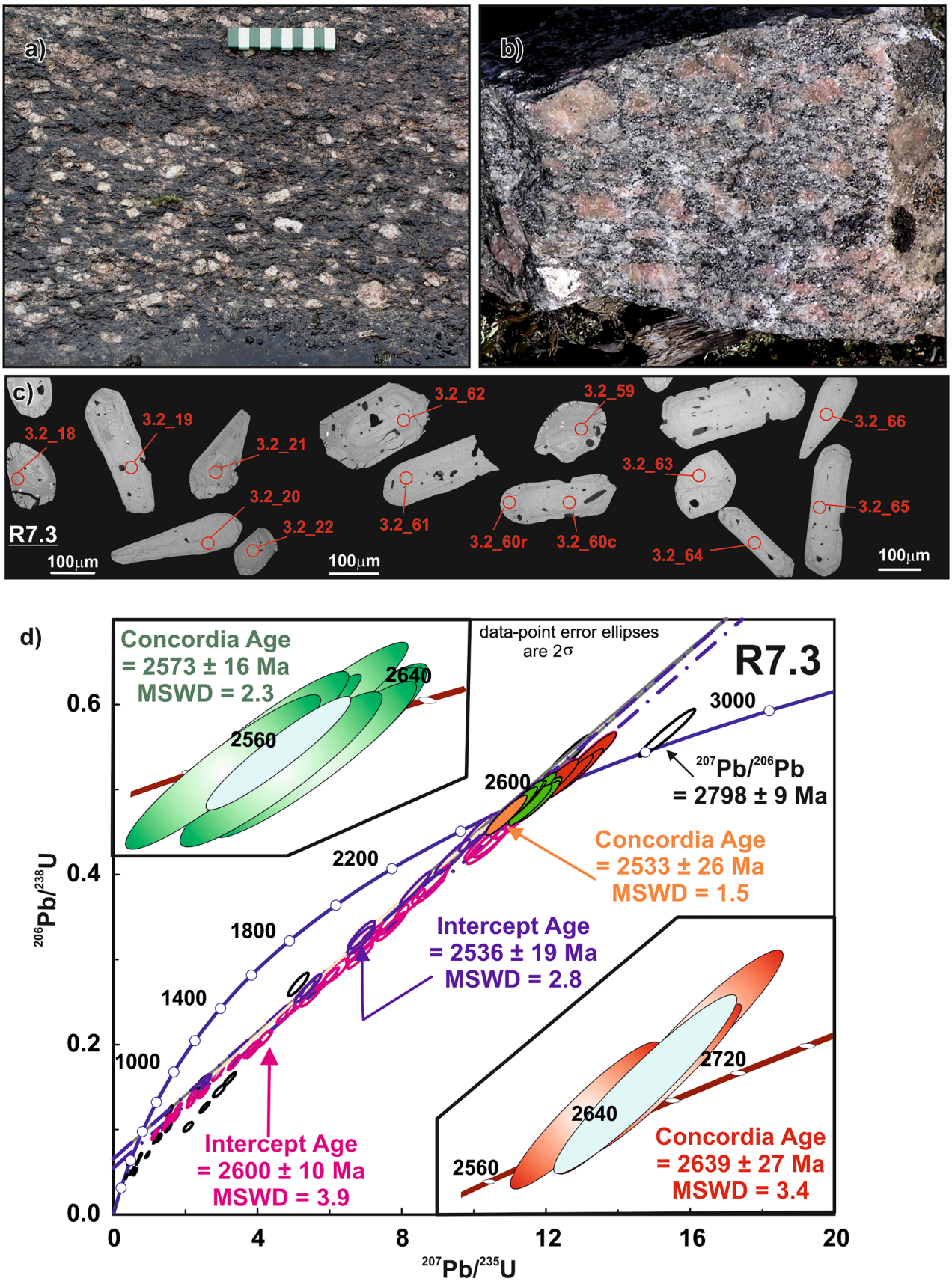

Fig. 6. Sample R7.3 (03.2), porphyritic granitoid, Näätämö, **(a)** outcrop (length of scale 10 cm), **(b)** sample (diameter 25 cm), **(c)** zircon BSE image, **(d)** U–Pb concordia plot. Location 69°39.101′N, 29°04.072′E.

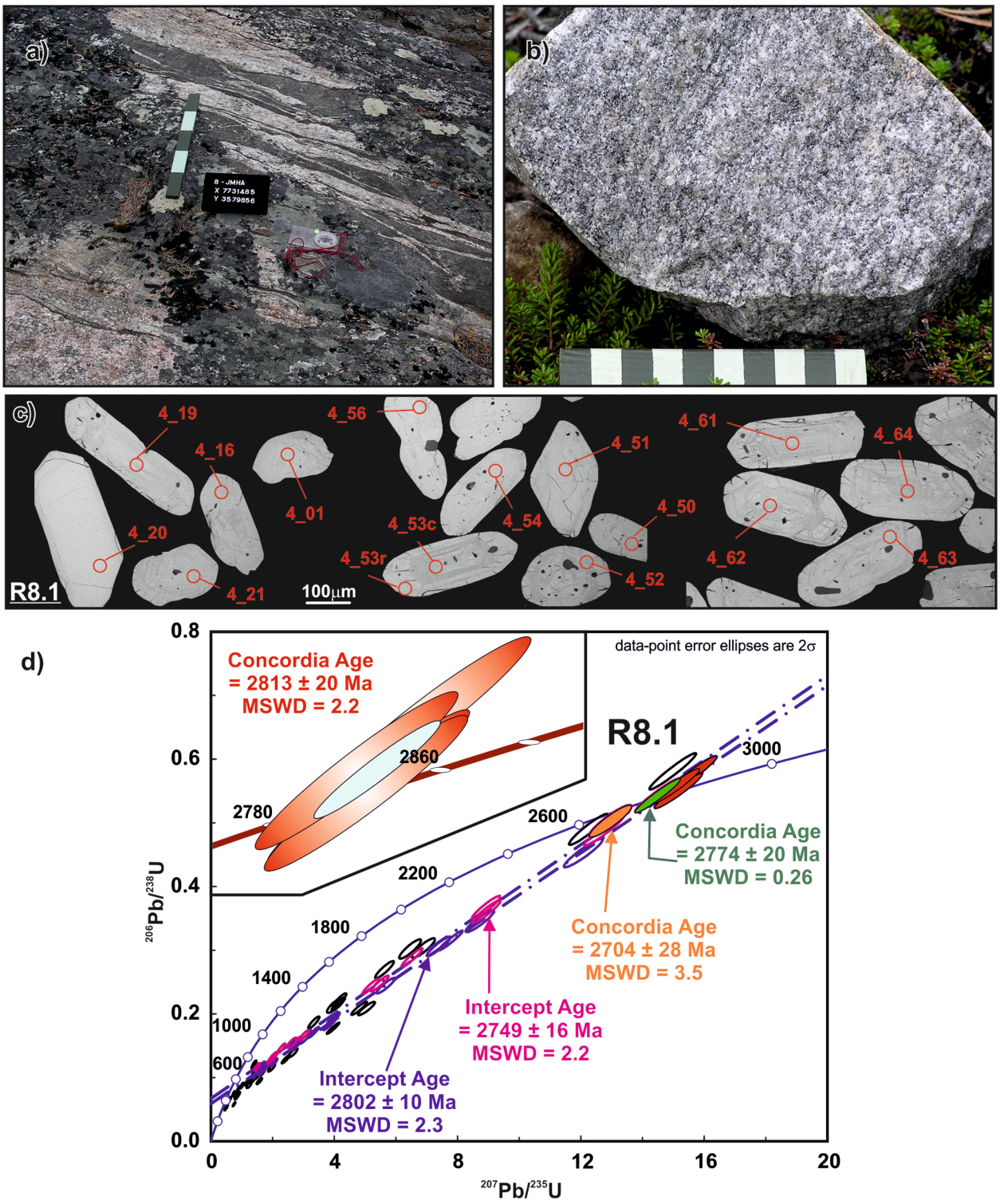

Fig. 7. Sample R8.1, high-HREE tonalite (04) Jääjärvi, **(a)** outcrop (length of scale 50 cm), **(b)** sample (length of scale 10 cm), **(c)** zircon BSE image, **(d)** U– Pb concordia plot. Location 69°39.042′N, 29°03.164′E.

melt sources may have existed in the Archaean.

The main phase of activity recorded by the Lake Inari zircons started at ca. 2900 Ma and continued seemingly without interruption until 2600 Ma, almost 300 million years (Fig. 9a). The prolonged period of the Lake Inari migmatization may thus represent a tectonic context associated with a stagnant mantle plume with restricted relative movement between the plume and the overlying lithosphere (Halla et al., 2024). The continued heating episode caused melting of metabasalts until the emplacement of porphyritic granitoids at 2.6–2.5 Ga indicating partial melting of TTGs at the end of the life cycle of the mantle plume.

5.3. Comparison of the ages of the low- and high-HREE TTGs

The Lake Inari TTGs form two geochemically distinct groups with differences especially in their HREE and MgO contents (Halla et al., 2024). Some earlier studies have suggested that the variation of HREE

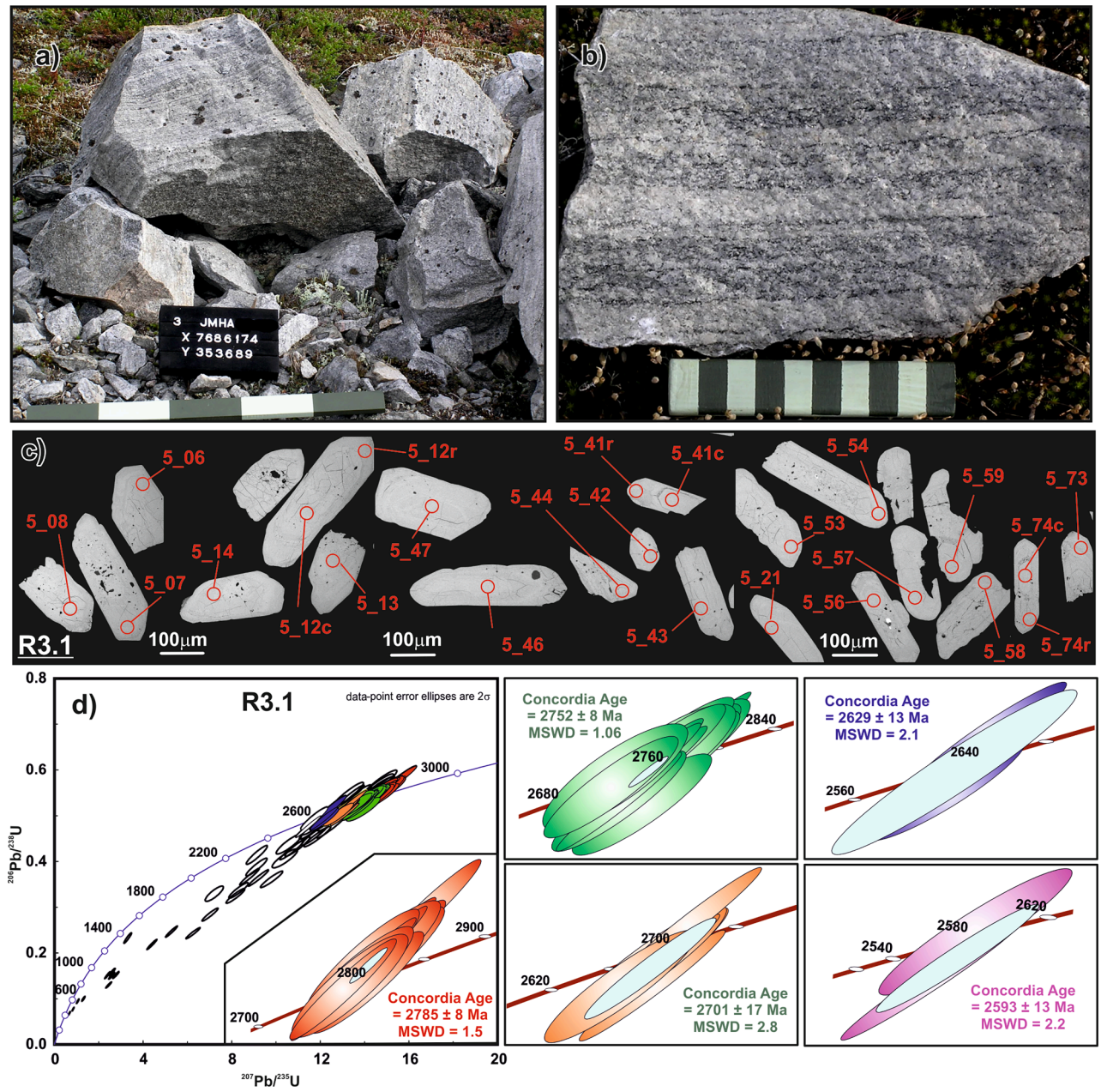

Fig. 8. Sample R3.1 (05) low-HREE tonalite, Aitajärvet, **(a)** outcrop (length of scale 50 cm), **(b)** sample (length of scale 10 cm), **(c)** zircon BSE image, **(d)** U– Pb concordia plot. Location 69° 15.242′N, 27° 55.719′E.

and MgO contents in TTGs is a time-dependent feature that reflects a secular change from flat to deep subduction (Martin and Moyen, 2002). However, later studies have advocated that the time correlation does not exist, and both geochemical groups have been found in formations of the same age (Halla, 2018; Halla et al., 2009, 2024; Mitra et al., 2019; Moyen, 2011). According to more recent research, the variation in TTGs may be the consequence of either magma hybridization, the mixing of several melt fractions throughout the ascent through the crust, or crustal differentiation of tonalitic magma (Laurent et al., 2020; Hernández--Montenegro et al., 2021). Halla et al. (2024) suggested that the variable geochemical signatures of the Lake Inari TTGs reflect internal magmatic processes and mingling of magmas that have experienced different evolutionary paths in terms of source mineralogy, degree of partial melting, fractionation and migration. Although the existence of the two geochemical endmembers in a spectrum of REE patterns is well confirmed, the reasons for their formation have remained unclear. The mode of occurrence of the two TTG types, i.e., their relationships, distribution and age, gives information on their tectonic setting.

Dating the two geochemical endmembers of TTGs sheds light on their temporal and spatial relations. Coeval and intermingled TTG groups would suggest common formation such as by partial melting at different stratigraphic positions of the same source, such as an oceanic plateau. Spatially and temporally distinct groups could, instead, indicate melting in completely different tectonic sites such as the lower part of the crust or subducting slab at shallow depths.

The studied zircon populations from the Lake Inari terrain show a large spread of ages from 3074 Ma to Paleoproterozoic (Fig. 9a–l). Table 4 presents the analysed $^{207}Pb/^{206}Pb$ zircon ages in terms of the number of grains/spots falling in time slots of 50 Ma. We found the oldest $^{207}Pb/^{206}Pb$ age of 3074 ± 9 Ma among the zircon population of the Näätämö low-HREE diatexite (Fig. 9c,i) from an outcrop enclosing metabasalts and being close to younger porphyritic granitoids. Most of

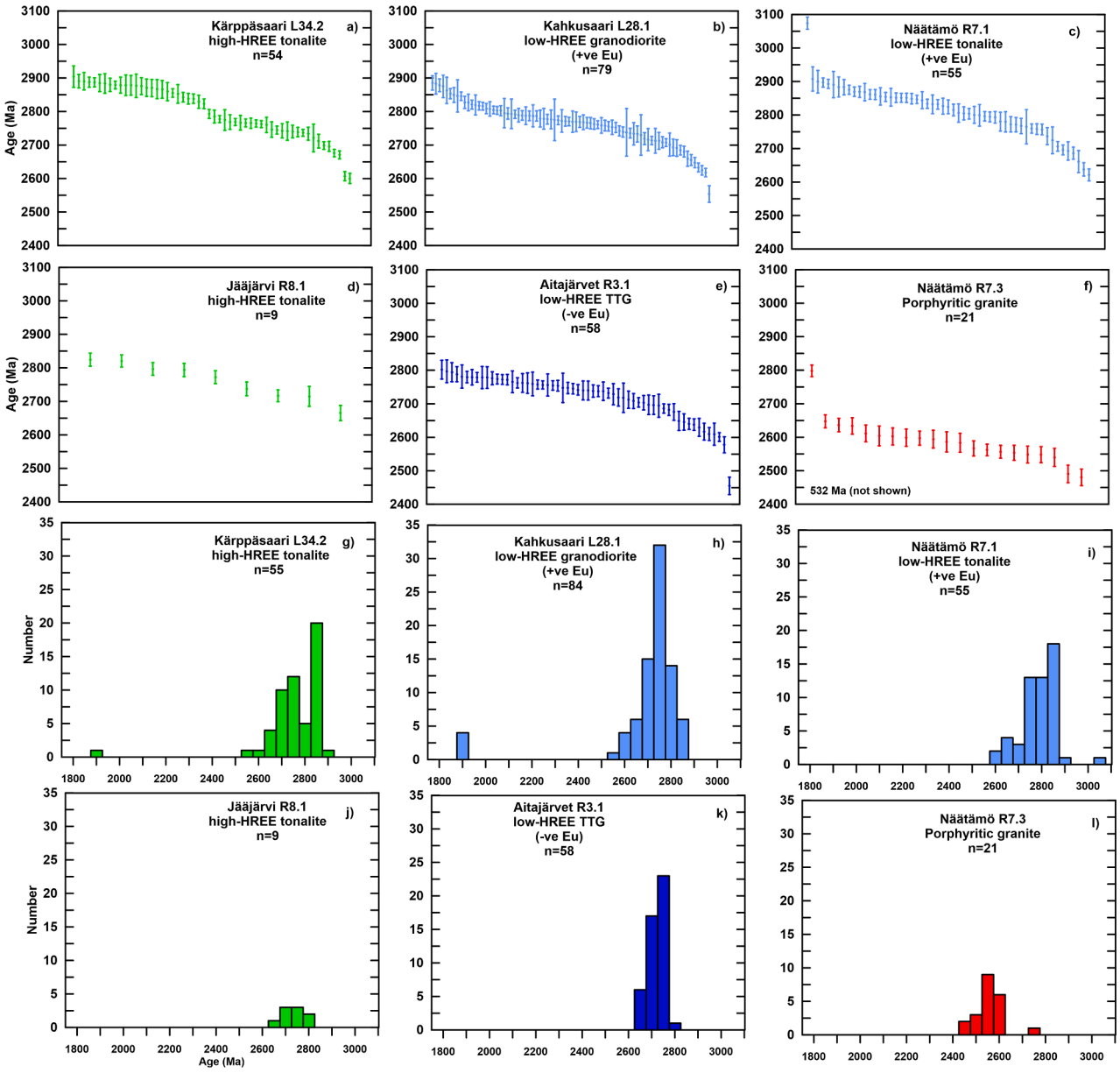

Fig. 9. (a-f) $^{207}Pb/^{206}Pb$ zircon ages (>90 % concordant) for the TTG samples from the Lake Inari terrain. **(g-l)** Histogram of the $^{207}Pb/^{206}Pb$ ages. Ages less than 1800 Ma not shown.

the other grains fall within the time window of 3000–2750 Ma. We identified an age of 2904 ± 16 Ma within the zircons from a high-HREE tonalite (Fig. 9a,g) from the Kärppäsaari Island. Zircons from both low- and high-HREE TTGs well occupy the time slot of 3000–2850 and a large share of the grains falls within the time slot of 2850–2800 Ma. This emphasizes the lack of temporal correlation within the different TTG-types. Some zircons from the Kahkusaari low-HREE TTG (Fig. 9b,h) fall well within the time window 3000–2800, but most of the grains fall in the slightly younger time window of 2800–2700 Ma. The Jääjärvi high-HREE (Fig. 9d,j) and Aitajärvet low-HREE tonalites (Fig. 9e,k) collected along the Kaamanen–Näätämö road show similar spread of ages mostly falling within the time window of 2800–2700 Ma.

Fig. 10 illustrates the relations of the HREE contents and ages. Fig. 10a–d shows the average REE patterns for different HREE types and porphyritic granitoids and Fig. 10e the age vs. total HREE plots for the samples. Our results show parallel chronology (Fig. 11) and confirm that the low- and high-HREE TTGs do not form temporally distinctive groups based on geochronology. The coeval and intermingled TTG types of the Lake Inari terrain can be explained by internal magmatic processes and mingling of magmas experienced different paths of differentiation and migration.

5.4. *Eastern and western tectonic blocks*

The FIRE 4A seismic reflection profile from Kaamanen to Näätämö runs along the road 971 and reflects the suture zone between the Karelia and Kola cratons (Patison et al., 2006). Two distinct blocks are identified in the profile, the eastern (ETB) and western (WTB) tectonic blocks. We analysed TTG samples from both the blocks but did not detect any significant differences in their age and geochemistry. The Jääjärvi (Fig. 9d, j) high-HREE TTG collected from the ETB shows parallel spread of ages to the Aitajärvet (Fig. 9e,k) low-HREE TTG from the WTB mostly falling within the time interval 2800–2700 Ma. The Näätämö low-HREE TTG shows parallel ages with the Kärppäsaari high-HREE TTG in the lake area. Our conclusion is that we are not able to tell the difference between the ETB and WTB based on geochronology. However, our results provide

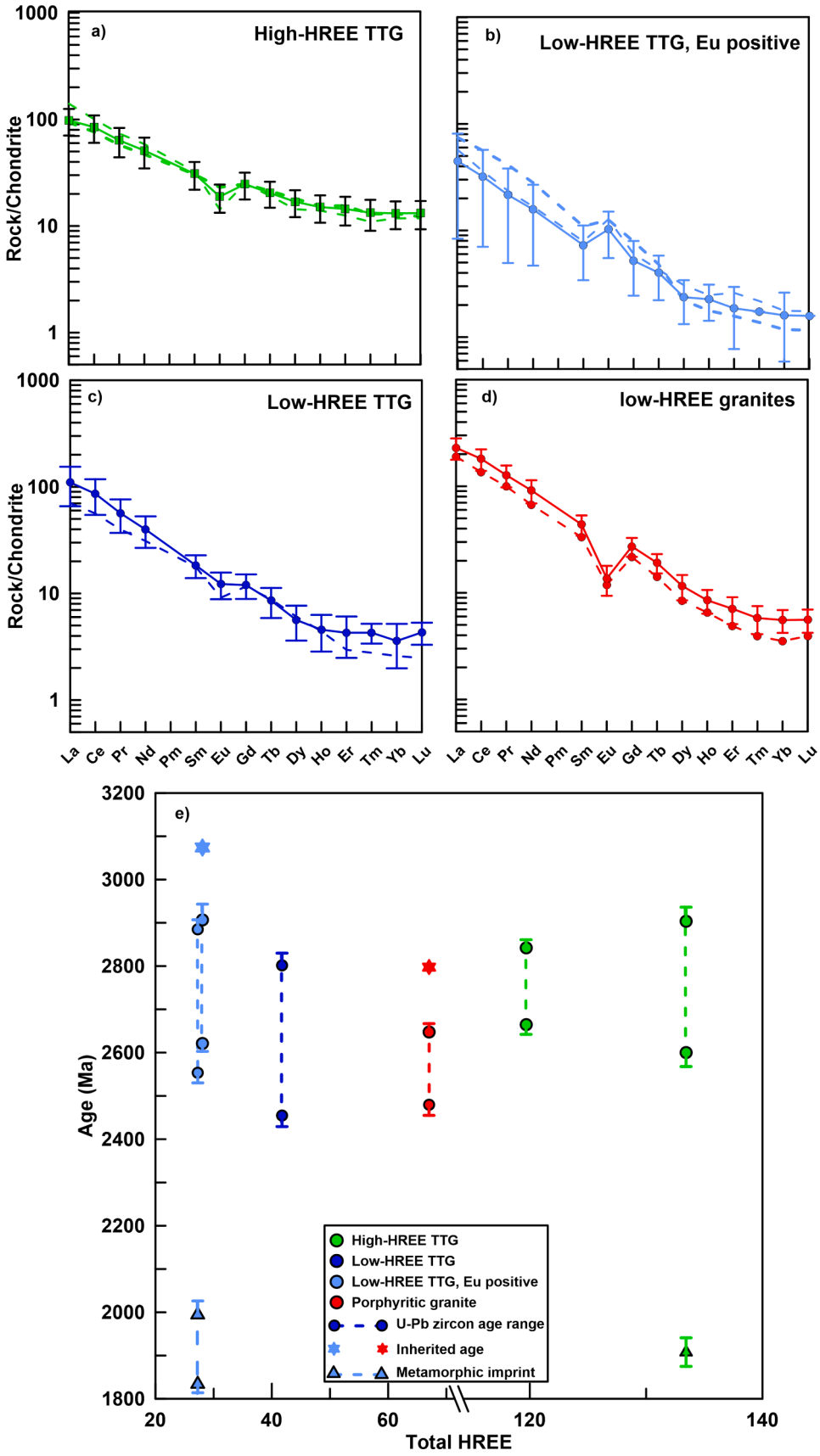

Fig. 10. (a). Average REE patterns of the studied TTGs and porphyritic granites. The vertical error bars show the standard deviation in the data. The dated samples are shown as dotted lines. **(b)** A $^{207}Pb/^{206}Pb$ age vs. total HREE plot for the analysed samples.

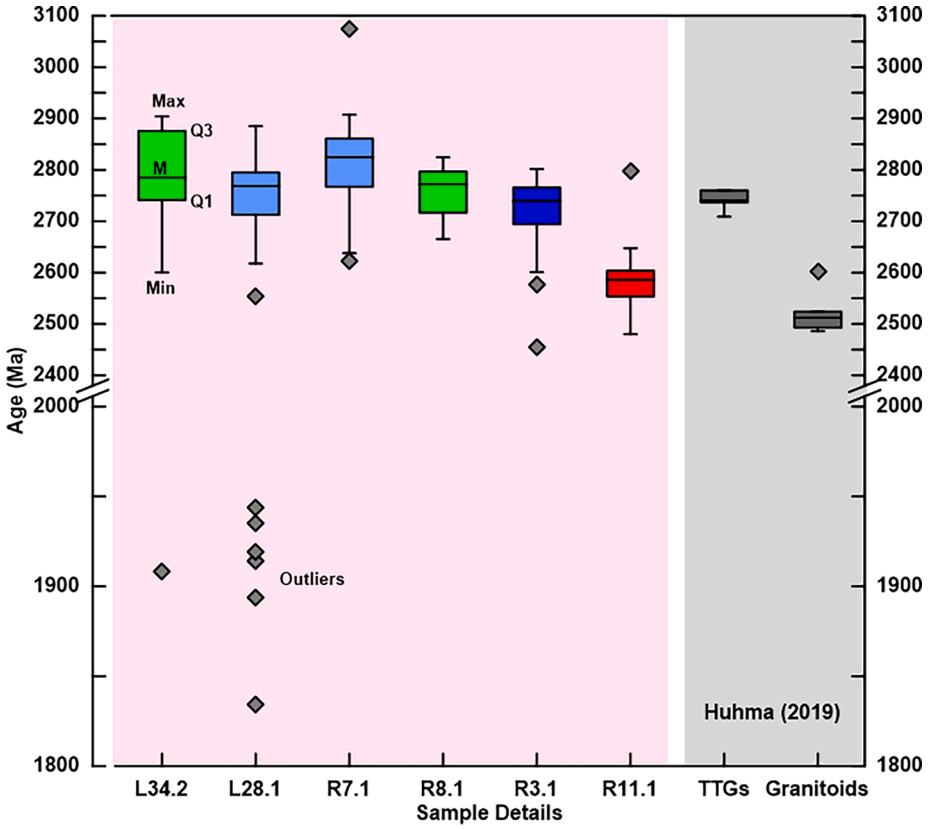

Fig. 11. Whisker plot for $^{207}Pb/^{206}Pb$ Ages (data from this study; Huhma, 2019) from the Lake Inari terrain. M: median, Q1: first quartile, Q3: third quartile. Min: minimum value in the dataset; Max: maximum value in the dataset; Outliers: low outliers are below Q1-1.5*IQR and above Q3-1.5*IQR. IQR = Q3-Q1.

new geochronological information for the FIRE 4A line interpretations. The rocks in the northernmost part of the profile have been previously regarded solely as around 2.6 Ga granitoids but our results show that TTGs with the oldest Archaean ages in the Lake Inari terrain, up to 3000 Ma, are found in the Näätämö area.

5.5. Chronology of the Lake Inari terrain

The protracted crystallization of zircons in the Lake Inari terrain has recorded many magmatic pulses and tectonothermal events related to the formation of the Lapland-Kola Province. The distribution of the age data from the Lake Inari terrain is summarized in a Whisker plot in Fig. 11. Our new geochronological results differ to some extent from those of the previous research on the Lapland-Kola province (Huhma, 2019; Lahtinen and Huhma, 2019) that suggested a more restricted time window of 2.76–2.71 Ga for the TTG formation (Table 1) and ages for granitoids extending from 2.60 to 2.49 Ga. The restricted time window for TTGs may be because many old analyses were carried out from bulk zircons fractions by TIMS (Thermal Ionization Mass Spectrometer) or just a matter of sampling bias.

Our new LA-ICP-MS results of U–Pb analyses on single zircons suggest a more protracted history for the partial melting processes that formed the Lake Inari terrain. The Zircon U–Pb concordia (Table 3) and $^{207}Pb/^{206}Pb$ (Table 4, Supplementary Table 8) ages from the Lake Inari terrain mainly spread from 2900 Ma to 2600 Ma (Fig. 9a) pointing to rather continuous evolution of 300 million years. We interpret the time interval 2900–2700 Ma as the main migmatization event that formed the metatexite, metatexite-diatexite transition and diatexite zones (Halla et al., 2024). During 200 million years the basaltic crust developed a buoyant TTG horizon that, eventually, started to partially melt to produce high-K granitoids. The formation of the Lake Inari terrain culminated between 2.6–2.5 Ga by the partial melting of TTGs to form porphyritic granitoids. This event is widely recorded in the zircons from the Lake Inari terrain indicating that the crust was thick enough for crustal anatexis to occur.

The formation of the LGB during the Lapland-Kola orogeny (Daly et al., 2006; Lahtinen and Huhma, 2019) is recorded only in the samples from Kahkusaari and Kärppäsaari, possibly because of their location closest to the LGB. The former shows the youngest U–Pb concordia age of 1.92 Ga from three analysed spots from the zircon rim (Table 3) and Pb–Pb age of 1.9 Ga for one spot (Table 4), the latter Pb–Pb ages spreading from 1.94–1.83 Ga (Table 4, Supplementary Table 8). We conclude that the ca. 1.9 Ga metamorphism associated with the formation of the LGB and Inari Arc caused minor zircon recrystallization in the Lake Inari terrain, but it did not influence its morphology. The latest event in the Lake Inari terrain is the formation of the Nattanen-type granite at 1.77 Ga (Heilimo et al., 2009, 2014). This event has not been directly recorded by the zircons but may have affected the < 2.5 Ga ages through Pb loss in samples that are closer to this granite.

5.6. Constraints to global Archaean crust-formation

The peaks in crust formation often correlates with the formation of major known supercontinents. Compared with the Proterozoic and Phanerozoic cyclic supercontinent formation and breakup producing few significant peaks of crustal growth, the Archaean crust formation was more continuous, albeit episodic (Joshi et al., 2022a). TTGs were formed every 0.1 Ga between 4.0 and 2.5 Ga, indicating a different geodynamic setting with more frequent but lower crustal growth peaks. This indicates a critical change in the Earth's geodynamics. Here, we concentrate on the time window 2900–2500 Ma, which is the time interval for the Archaean magmatic and tectonothermal activity of the Lake Inari terrain. Fig. 12a shows a KDE (Kernel density estimate) plot visualizing the distribution of the Lake Inari ages with respect to global

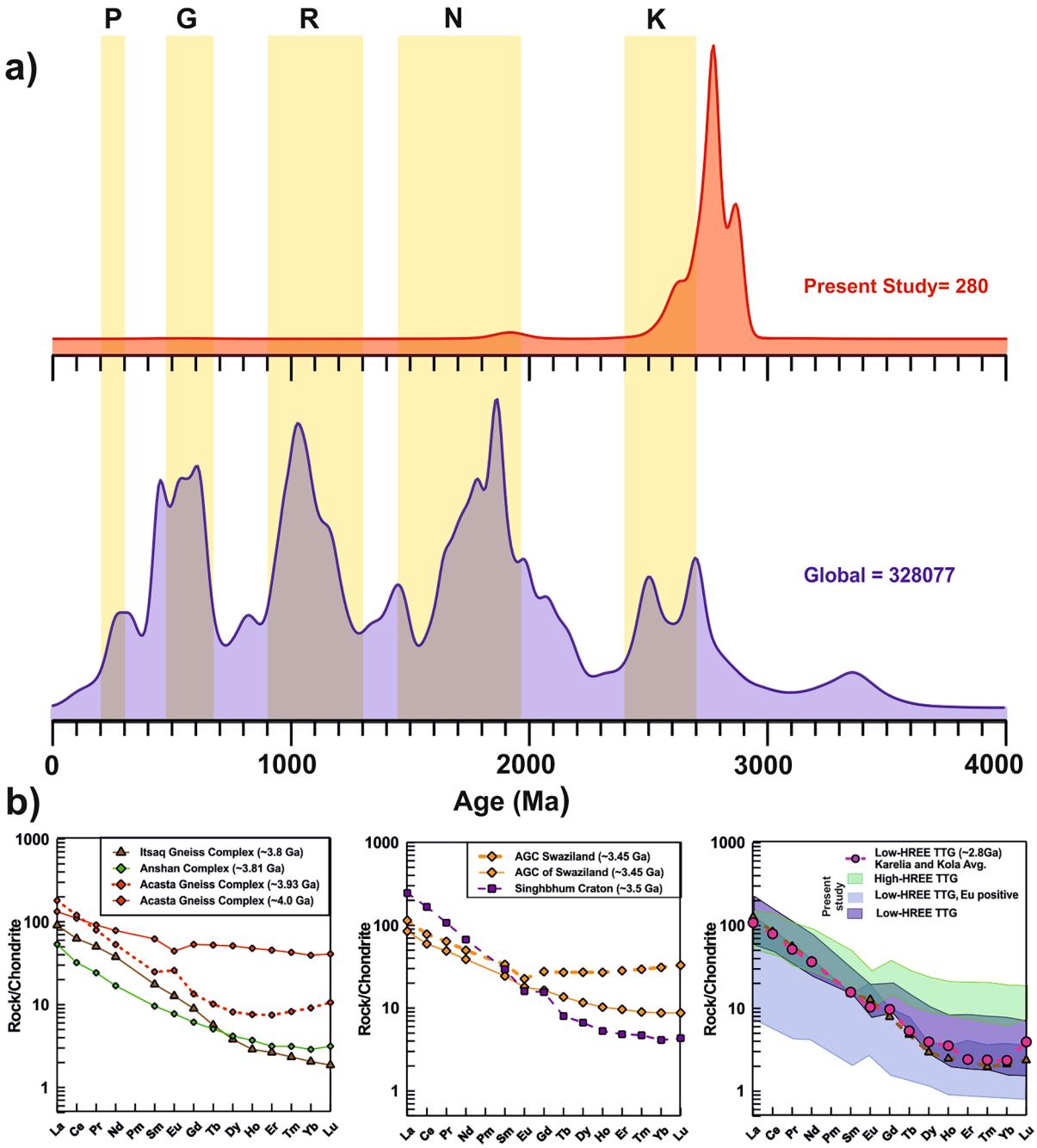

Fig. 12. **(a)** KDE plots of global detrital zircon population (in blue) compared with the U–Pb ages from the Lake Inari TTGs (orange). The yellow bands depict the ages of supercontinent assembly (after Barham et al., 2019 and references therein). P: Pangea; G: Gondwanaland; R: Rodinia; N: Nuna/Columbia; K: Kenorland. Only ages with 90% or more concordance are plotted. **(b)** REE patterns of Eoarchaean (left), Paleoarchaean (middle), and Meso- to Neoarchaean (right) TTGs. Data compiled by Halla (2018).

crustal growth and supercontinent formation based on detrital zircons (e.g., Joshi et al., 2022a and references therein). Based on the diagram, it seems that the crustal growth in the Lake Inari peaks at approximately 2.8 Ga, i.e., 100 Ma before the peak in the formation of the alleged Kenorland supercontinent at 2.7 Ga.

Fig. 12b illustrates the occurrence of different types of TTGs through time by comparing REE patterns of Eoarchaean, Paleoarchaean and Meso- to Neoarchaean TTGs selected from the literature (data and references in Halla, 2018). The Earth's earliest tonalites, the Eoarchaean Idiwhaa tonalites of the Acasta gneisses in the Slave Province, show high-HREE contents suggesting shallow melting within Hadean mafic crust at around 4.0 Ga. The Eoarchaean Acasta (Slave Province), Itsaq (southern West Greenland) and Anshan (North China Craton) TTGs represent the earliest low-HREE TTGs. In the Paleoarchaean, both low- and high-HREE TTGs were formed in the Singhbhum (eastern India) and Swaziland cratons and their formation continued to Mesoarchaean as evidenced by the Yangtze TTGs (North China Craton). The formation of both low- and high-HREE TTGs continued until the Neoarchaean, as shown by the 2800–2700 Ma Fennoscandian high- and low-HREE averages and our new results from the Lake Inari terrain. In conclusion, our study confirms that the formation of the high- and low-HREE TTGs is not time-dependent, and that the Lake Inari terrain cannot yet be identified as a part of any Archaean supercontinent, although its formation overlaps with a peak in global TTG formation.

6. Conclusions

Based on our studies on the Lake Inari terrain, we conclude the following:

1. The large time spread in zircon populations suggest a prolonged magmatic activity in the TTG terrain from 2900 to 2600 Ma, supporting a protracted and stationary source of heat such as a stagnant mantle plume with restricted relative movement between the plume and the overlying lithosphere.
2. The high-HREE and low-HREE TTGs show parallel ages and are intermingled, pointing to a common, geochemically heterogeneous source instead of different tectonic settings.
3. There is no distinct age difference between the eastern and western tectonic blocks identified in the FIRE (Finnish Reflection Experiment) 4A seismic reflection lines. The oldest ages are found in the eastern block.
4. The coeval and intermingled TTG types of the Lake Inari terrain can be explained by internal magmatic processes and mingling of magmas experienced different paths of differentiation and migration. Prolonged melting episodes in thickened TTG crust produced porphyritic granites between 2650–2500 Ma.
5. The Lake Inari crustal growth peaks approximately at 2.8 Ga, i.e., 100 Ma before the peak in the formation of the suggested Kenorland supercontinent at 2.7 Ga.

CRediT authorship contribution statement

Kumar Batuk Joshi: Writing – original draft, Visualization, Investigation, Formal analysis, Conceptualization. **Jaana Halla:** Writing – review & editing, Writing – original draft, Resources, Project administration, Investigation, Funding acquisition, Conceptualization. **Matti Kurhila:** Writing – original draft, Supervision, Methodology, Investigation, Formal analysis, Data curation, Conceptualization. **Esa Heilimo:** Writing – original draft, Supervision, Resources, Investigation, Conceptualization.

Declaration of competing interest

The authors declare that they have no known competing financial interests or personal relationships that could have appeared to influence the work reported in this paper.

Data availability

The data is available online as supplementary material of this paper.

Acknowledgements

We acknowledge the support from the K.H. Renlund Foundation and thank Kristopher Szilas and Richard Palin for their constructive reviews which helped us to crystallize our thoughts and significantly improve the manuscript. We greatly appreciate the competent guidance of Teemu Vehkamäki in the zircon separation process. We are also thankful for Satu and Ville Kurunsaari for taking care of our boating and camping logistics on the Lake Inari.

Appendix A. Supplementary material

Supplementary data to this article can be found online at https://doi.org/10.1016/j.precamres.2024.107418.

References

Barham, M., Kirkland, C.L., Hollis, J., 2019. Spot the difference: zircon disparity tracks crustal evolution. Geology 47, 435–439. https://doi.org/10.1130/G45840.1.

Chen, Z., Liu, Y.-J., Chen, G.-N., Peng, Z.-L., 2017. Rheological transitions in progressive melting of rock and their geological constraints from the Fuhu metatexite-diatexite profile in Guangdong Province, SE China. J. Asian Earth Sci. 139, 192–201. https://doi.org/10.1016/j.jseaes.2017.02.009.

Chen, L., Wang, X., Liang, X., Wan, B., Liun, L., 2020. Subduction tectonics vs. plume tectonics—Discussion on driving forces for plate motion. Sci. China Earth Sci. 3, 315–328. https://doi.org/10.1007/s11430-019-9538-2.

Cisneros de León, A., Schmitt, A.K., Kutterolf, S., Schindlbeck-Belo, J.C., Hernández, W., Sims, K.W.W., Garrison, J., Kant, L.B., Weber, B., Wang, K.L., Lee, H.Y., 2021. Zircon and melt extraction from a long-lived and vertically extensive magma system underneath Ilopango Caldera (El Salvador). Geochem. Geophys. Geosyst. 22 (5), e2020GC009507.

Condie, K.C., Puetz, S.J., Spencer, C.J., Roberts, N.M.W., 2024. Four billion years of secular compositional change in granitoids. Chem. Geol. 644 https://doi.org/10.1016/j.chemgeo.2023.121868.

Daly, J.S., Balagansky, V.V., Timmerman, M.J., Whitehouse, M.J., 2006. The Lapland Kola orogen: Palaeoproterozoic collision and accretion of the northern Fennoscandian lithosphere. In: Gee, D.G., Stephenson, R.A. (Eds.), European Lithosphere Dynamics. Geological Society, London, Memoirs, pp. 561–578.

Debon, F., Le Fort, P., 1983. A chemical-mineralogical classification of common plutonic rocks and associations. Trans. R. Soc. Edinb. Earth Sci. 73, 135–149.

DeCelles, P.G., Ducea, M.N., Kapp, P., Zandt, G., 2009. Cyclicity in Cordilleran orogenic systems. Nat. Geosci. 2 (4), 251–257.

Ducea, M.N., Paterson, S.R., DeCelles, P.G., 2015a. High-volume magmatic events in subduction systems. Elements 11 (2), 99–104.

Ducea, M.N., Saleeby, J.B., Bergantz, G., 2015b. The architecture, chemistry, and evolution of continental magmatic arcs. Annu. Rev. Earth Planet. Sci. 43, 299–331.

Halla, J., 2018. Highlights on geochemical changes in Archaean Granitoids and their implications for early earth geodynamics. Geosciences 8 (9), 353. https://doi.org/10.3390/geosciences8090353.

Halla, J., 2020. The TTG-amphibolite terrains of arctic fennoscandia: infinite networks of amphibolite metatexite-diatexite transitions. Front. Earth Sci. 8, 252. https://doi.org/10.3389/feart.2020.00252.

Halla, J., Joshi, K.B., Luttinen, A., Heilimo, E., Kurhila, M., 2024. On the origin of Archaean TTGs by migmatization of mantle plume-related metabasalts: Insights from the Lake Inari terrain, Arctic Fennoscandia. Precambr. Res. 407, 107407.

Halla, J., van Hunen, J., Heilimo, E., Hölttä, P., 2009. Geochemical and numerical constraints on Neoarchean plate tectonics. Precambr. Res. 174, 155–162. https://doi.org/10.1016/j.precamres.2009.07.008.

Heilimo, E., Halla, J., Lauri, L.S., Rämö, O.T., Huhma, H., Kurhila, M.I., Front, K., 2009. The Paleoproterozoic Nattanen-type granites in northern Finland and vicinity – a postcollisional oxidized A-type suite. Bull. Geol. Soc. Finl. 81, 7–36. https://doi.org/10.17741/bgsf/81.1.001.

Heilimo, E., Elburg, M., Andersen, T., 2014. Crustal growth and reworking during Lapland-Kola orogeny in northern Fennoscandia: U-Pb and Lu-Hf data from the Nattanen and Litsa-Aragub-type granites. Lithos 205, 112–126. https://doi.org/10.1016/j.lithos.2014.06.014.

Hernández-Montenegro, J.D., Palin, R.M., Zuluaga, C.A., Hernández-Uribe, D., 2021. Archean continental crust formed by magma hybridization and voluminous partial melting. Sci. Rep. 11 (1), 5263.

Horstwood, M.S.A., Košler, J., Gehrels, G., Jackson, S.E., McLean, N.M., Paton, C., Pearson, N.J., Sircombe, K., Sylvester, P., Vermeesch, P., Bowring, J.F., Condon, D.J., Schoene, B., 2016. Community-derived standards for LA-ICP-MS U-(Th-)Pb geochronology—Uncertainty propagation, age interpretation and data reporting. Geostand. Geoanal. Res. 40, 311–332.

Huhma, H., Mänttäri, I., Peltonen, P., Kontinen, A., Halkoaho, T., Hanski, E., Hokkanen, T., Hölttä, P., Juopperi, H., Konnunaho, J., Layahe, Y., Luukkonen, E., Pietikäinen, K., Pulkkinen, A., Sorjonen-Ward, P., Vaasjoki, M., Whitehouse, M., 2012. The age of the Archaean greenstone belts in Finland. Geol. Surv. Finland Spec. Pap. 54, 74–175.

Huhma, H., 2019. Isotope results from Lapland-Kola province in Finland. Geological Survey of Finland, Open file research report 37 https://tupa.gtk.fi/raportti/arkisto/37_2019.pdf.

Johnson, T., Yakymchuk, C., Brown, M., 2021. Crustal melting and suprasolidus phase equilibria: From first principles to the state-of-the-art. Earth Sci. Rev. 221, 103778.

Joshi, K.B., Bhattacharjee, J., Rai, G., Halla, J., Ahmad, T., Kurhila, M., Heilimo, E., Choudhary, A.K., 2017. The diversification of granitoids and plate tectonic implications at the Archaean-Proterozoic boundary in the Bundelkhand Craton, Central India. Geol. Soc. Lond. Spec. Publ. 449 (1), 123–157.

Joshi, K.B., Banerji, U.S., Dubey, C.P., Oliveira, E.P., 2022a. Detrital Zircons in Crustal Evolution: A Perspective from the Indian Subcontinent. Lithosphere 2022 (Special 8), 3099822. https://doi.org/10.2113/2022/3099822.

Joshi, K.B., Singh, S.K., Halla, J., Ahmad, T., Rai, V.K., 2022b. Neodymium Isotope constraints on the origin of TTGs and High-K Granitoids in the Bundelkhand Craton, Central India: implications for Archaean crustal evolution. Lithosphere 2022 (Special 8), 6956845. https://doi.org/10.2113/2022/6956845.

Joshi, K.B., Sorcar, N., Pant, N.C., Nandakumar, V., Ahmad, T., Tomson, J.K., 2021. Characterization of multiple episodes of melt generation from lower crust during Archaean using amphibole composition. Episodes J. Int. Geosci. 44 (4), 443–466.

Lahtinen, R., Huhma, H., 2019. A revised geodynamic model for the Lapland-Kola orogen. Precambr. Res. 330, 1–19. https://doi.org/10.1016/j.precamres.2019.04.022.

Laurent, O., Björnsen, J., Wotzlaw, J.F., Bretscher, S., Pimenta Silva, M., Moyen, J.F., Ulmer, P., Bachmann, O., 2020. Earth's earliest granitoids are crystal-rich magma reservoirs tapped by silicic eruptions. Nat. Geosci. 13, 163–169.

Li, Z., Shan, X., Liu, J., Zhang, J., Liu, Z., Cheng, C., Wang, Z., Zhao, C., Yu, H., 2023. Late Neoarchean TTG and monzogranite in the northeastern North China Craton: Implications for partial melting of a thickened lower crust. Gondw. Res. 115, 201–223. https://doi.org/10.1016/j.gr.2022.10.008.

Ludwig, K.R., 2012. User's Manual for Isoplot 4.15, A Geochronological Toolkit for Microsoft Excel. Berkeley, CA: Berkeley Geochronology Center Special Publication no. 5, 75p.

Martin, H., Moyen, J.-F., 2002. Secular changes in TTG composition as markers of the progressive cooling of the Earth. Geology 30, 319–322. https://doi.org/10.1130/00917613(2002)030%3C0319:SCITTG%3E2.0.CO;2.

Meriläinen, K., 1976. The granulite complex and adjacent rocks in Lapland, northern Finland. Bull. Geol. Soc. Finl. 289, 129 pp.

Mitra, A., Dey, S., Zong, K., Liu, Y., Mitra, A., 2019. Building the core of a Paleoarchean continent: Evidence from granitoids of Singhbhum Craton, eastern India. Precambr. Res. 335, 105436.

Moyen, J.-F., 2011. The composite Archaean grey gneisses: Petrological significance, and evidence for a non-unique tectonic setting for Archaean crustal growth. Lithos 123, 1–36. https://doi.org/10.1016/j.lithos.2010.09.015.

Moyen, J.F., Martin, H., 2012. Forty years of TTG research. Lithos 148, 312–336. https://doi.org/10.1016/j.lithos.2012.06.010.

Müller, W., Shelley, M., Miller, P., Broude, S., 2009. Initial performance metrics of a new custom-designed ArF excimer LA-ICPMS system coupled to a two-volume laser-ablation cell. J. Anal. At. Spectrom 24, 209–214.

Nagel, T.J., Hoffmann, J.E., Münker, C., 2012. Generation of Eoarchean tonalite-trondhjemite-granodiorite series from thickened mafic arc crust. Geology 40 (4), 375–378.

Naif, S., Miller, N.C., Shillington, D.J., Bécel, A., Lizarralde, D., Bassett, D., Hemming, S. R., 2023. Episodic intraplate magmatism fed by a long-lived melt channel of distal plume origin. Sci. Adv. 9 (23), eadd3761.

Patchett, J., Kouvo, O., 1986. Origin of continental crust of 1.9-1.7 Ga age: Nd isotopes and U-Pb zircon ages in the Svecokarelian terrain of south Finland. Contrib. Miner. Petrol. 92, 1–12.

Patison, N.L., Korja, A., Lahtinen, R., Ojala, V.J., the FIRE working Group, 2006. FIRE seismic reflection profiles 4, 4A and 4B: Insights into the Crustal Structure of Northern Finland from Ranua to Näätämö. Geological Survey of Finland, Special Paper 43, 161–222. https://tupa.gtk.fi/julkaisu/specialpaper/sp_043_pages_161_222.pdf.

Rollinson, H.R., 2023. The growth of the Zimbabwe craton during the Neoarchaean. Contribut. Mineral. Petrol. 178 https://doi.org/10.1007/s00410-022-01978-7.

Sotiriou, P., Polat, A., Windley, B., Kusky, T., 2023. Temporal variations in the incompatible trace element systematics of Archean TTGs: Implications for crustal growth and tectonic processes in the early Earth. Earth Sci. Rev. 236, 104274 https://doi.org/10.1016/j.earscirev.2022.104274.

Stacey, J.S., Kramers, J.D., 1975. Approximation of terrestrial lead isotope evolution by a two-stage model. Earth Planet. Sci. Lett. 26, 207–221.

Tarduno, J.A., Cottrell, R.D., Bono, R.K., Rayner, N., Davis, W.J., Zhou, T., Nimmo, F., Hofmann, A., Jodder, J., Ibañez-Mejia, M., Watkeys, M.K., Oda, H., Mitra, G., 2023. Hadaean to Palaeoarchaean stagnant-lid tectonics revealed by zircon magnetism. Nature 618, 531–536. https://doi.org/10.1038/s41586-023-06024-5.

Taylor, R.J., Johnson, T.E., Clark, C., Harrison, R.J., 2020. Persistence of melt-bearing Archean lower crust for> 200 my—An example from the Lewisian Complex, northwest Scotland. Geology 48 (3), 221–225.

Tuisku, P., Mikkola, P., Huhma, H., 2006. Evolution of migmatitic granulite complexes: Implications from Lapland granulite belt, part I: Metamorphic geology. Bull. Geol. Soc. Finl. 78, 71–105. https://doi.org/10.17741/bgsf/78.1.004.

Van Achterbergh, E., Ryan C., Jackson, S., Griffin W., 2001. Data reduction software for LA-ICP-MS, in: Laser-Ablation ICPMS in the Earth Sciences – Principles and applications, Mineralogical Association of Canada short course series, 29, St John, Newfoundland, 239−243.

Weinberg, R.F., Hasalová, P., 2015. Water-fluxed melting of the continental crust: a review. Lithos 212, 158–188.